

SURFACE PLASMON PROPERTIES OF HOLLOW AUAG ALLOYED TRIANGULAR NANOBXES AND ITS APPLICATIONS IN SERS IMAGING AND POTENTIAL DRUG DELIVERY

X. W. Liu^{1,2}, J. Lin¹, T. F. Jiang¹, Z. F. Zhu¹, Q. Q. Zhan¹, J. Qian^{1,2}, and S. He^{1,2,*}

¹Centre for Optical and Electromagnetic Research, Zhejiang Provincial Key Laboratory for Sensing Technologies, Zhejiang University, Hangzhou 310058, China

²Joint Research Lab of Optics of Zhejiang Normal University and Zhejiang University, Hangzhou 310058, China

Abstract—We successfully synthesized hollow AuAg alloyed triangular nanobxes (TNBs) with localized surface plasmon resonances (LSPR) spectra position from visible to NIR region. We then study the surface plasmon properties of AuAg alloyed TNBs and explore their application in surface enhanced Raman scattering (SERS) imaging. We also investigated the laser induced near-field ablation of TNBs, which have the potentials of drug delivery for cancer treatment. Finite Difference Time Domain (FDTD) method is used to calculate electromagnetic fields induced by optical excitation of LSPR of AuAg alloyed TNBs for the first time. The calculated results are proved through in-vivo SERS imaging by three types of SERS tags based on TNBs. Furthermore, the unique hollow structure of TNBs may facilitate direct encapsulation of anticancer drugs, without any surface coatings. The femtosecond laser near-field ablation experiment is studied as one possible method to release the drug encapsulated inside the hollow structure. These studies show that the nanostructures are easy to break down and promising as a nanodevice model for controlled drug delivery.

Received 19 April 2012, Accepted 15 May 2012, Scheduled 15 May 2012

* Corresponding author: Sailing He (sailing@kth.se).

1. INTRODUCTION

Metal nanostructures have been studied intensively due to their fascinating electromagnetic properties [1–3] and versatile applications to nanodevices [4–7]. Among various systems, nonspherical Ag or Au nanoparticles have been widely used for bioimaging [8] and biosensing [9], due to the unique optical properties governed by the collective oscillation of the conductive electrons in resonance with certain frequencies of incident light, that is, localized surface plasmon resonance (LSPR). LSPR is strongly dependent on the size, shape, and composition of the nanoparticles, as well as the refractive index of the surrounding medium [10, 11]. Au, Ag and AuAg alloyed triangular nanoplates (NPs) have attracted a great deal of attention among researchers. Compared with Au or Ag nanospheres (NSs), NPs have several advantages due to their triangular plate shape. Firstly, the optical spectra of NPs usually show two resonance bands corresponding to in-plane dipole and quadrupole oscillations [12, 13]. The main LSPR band of NPs can be easily tuned from visible to near infrared (NIR) region by changing the aspect ratio of the lateral length to thickness [14, 15], which cannot be achieved in NSs [8]. Secondly, the LSPR sensitivity of NPs to the surrounding index is higher, due to the sharp geometries [1, 16]. Thirdly, it has been demonstrated that NPs show much stronger local field enhancement than NSs, both with discrete dipole approximation (DDA) calculations [17] and electron energy-loss spectroscopy (EELS) surface plasmon probing [18].

Recently, template techniques paved the way for researchers to synthesize some novel hollow nanostructures. The AuAg alloyed triangular nanobox (TNB), a complete AuAg alloyed shell with a hollow interior, has been fabricated based on an Ag nanoprism template [19]. UV-vis extinction spectra show that the optical decay (OD) of AuAg alloyed TNBs solution is larger than that of the original Ag NPs templates solution. Furthermore, the yield of TNBs is almost the same as Ag NPs (over 95% at room temperature [15]) and the synthesis process is simple and rapid (almost 30 mins). Third, the AuAg alloyed structures is more stable and biocompatible than Ag nanostructures [20, 21]. Finally, the unique hollow structure of AuAg alloyed TNBs is advantageous for applications such as controlled drug delivery. Hence, AuAg alloyed TNBs might be a better multifunctional platform for biosensing, biomedical imaging and even cancer therapy than Au and Ag NPs.

In this paper, we conducted a systematic study of surface plasmon properties of an AuAg alloyed triangular nanobox. We synthesized four types of nanoboxes with different dimensions and LSPR spectra

position from visible to NIR region. The finite-difference time-domain (FDTD) method was first used to investigate the electromagnetic fields induced by optical excitation of LSPR of TNBs, based on TEM data from the experiment. As the results show, TNBs produce a much larger electric field (E -field) enhancement than Au or Ag nanospheres. TNBs were then used to prepare a new kind of SERS tags. Three types of SERS tags based on 640 nm TNBs were successfully used in “in vivo” SERS detection. In addition, we first explore the potential applications of AuAg alloyed TNBs in drug delivery. The existence of the hollow cavity of TNBs may facilitate direct encapsulation of molecules and materials of interest without any surface coatings. We also found that laser ablation induced by femtosecond (fs) laser pulses is one possible way to release the drug inside the hollow structure.

2. METHODS AND MATERIALS

2.1. AuAg Alloyed TNBs Synthesis

AuAg alloyed TNBs were synthesized from Ag nanoprisms (NP) template.

2.1.1. Ag NPs Synthesis

AgNPs was fabricated with a seed mediated approach [15]. The seed was prepared by adding aqueous AgNO_3 (5 mL, 0.5 mM) into solution mixing aqueous trisodium citrate (5 mL, 2.5 mM), aqueous poly (sodium styrenesulphonate) (PSSS; 0.25 mL, 500 mg L^{-1}) and aqueous NaBH_4 (0.3 mL, 10 mM) at a rate of 2 mL min^{-1} , while continuously stirring for 20 mins. Four Ag NPs samples noted P1–P4 were synthesized by adding 400, 200, 100 and 20 μL seed solution into four 5 mL 15 nm ascorbic acid (AA), respectively. Then, 3 mL 0.5 mM AgNO_3 solution was added into these solutions at a rate of 1 mL min^{-1} while continuously stirring 3 mins later, the four Ag NPs samples with different dimensions were successfully synthesized.

2.1.2. AuAg Alloyed TNBs Synthesis

4.4 mL HAuCl_4 was added into 3 mL Ag NPs sample at a rate of 1 mL min^{-1} , following the addition of 360 μL 10 mM AA. Almost 5 mins later, AuAg alloyed TNBs formed and solutions derived from Sample P1–P4 were noted by B1–B4, respectively. Au/Ag ration of sample B1–B4 were all almost 4 : 1.

2.2. Surface Modification of AuAg Alloyed TNBs

Three kinds of dyes (DTTC, DTDC and O170) and PEG coated AuAg alloyed TNBs were synthesized with the same two-step process. First, 10 μL ethanol solution with 1 mm dye was quickly added into 1 mL prepared AuAg alloyed TNBs solution (sample B2) and vortexed for 1 min. Then, 100 μL 10 mg mL^{-1} thiol-PEG aqueous solution was added into dye-TNBs solution while vortexed for 1 min. After 2 h adsorption time, both dyes and thiol-PEG conjugated on the TNBs surface through Au/Ag-S bond [22, 23] to form dyes and PEG coated AuAg alloyed TNBs (PEG-DTTC-TNBs, PEG-DTDC-TNBs and PEG-O170-TNBs). The PEG-dye-TNBs solutions were centrifuged at 9000 rpm for 8 mins and redispersed into deionized water, solutions with different PH value, serum or PBS solution (1X, PH=7.4).

2.3. Characterization

The extinction spectra of all the samples were recorded with a UV-vis scanning spectrophotometer (Shimadzu 2550). The structure of Ag NPs and AuAg alloyed TNBs was imaged by a transmission electron microscope (TEM) (JEOL JEM-1200EX) operated at 160 kV in bright-field mode. The Raman spectra were measured with a Raman spectrometer (BWTEK) consisting of a Raman probe, laser source and spectrometer. Excitation light (785 nm, 300 mW) from the source was conducted by an excitation fiber and focused with a convex lens ($f = 7.5$ mm) onto the sample. The scattering light from the sample was collected through another fiber and sent to the spectrometer. A long pass filter was used to block the elastic scattering light and extract the Raman signal.

2.4. In Vivo SERS Detection

All in vivo experiments were executed under the requirements of Zhejiang University Animal Study Committee for the care and use of laboratory animals in research. Two 18–21 g male ruder mice were used for in vivo SERS experiment. Four locations on one mouse's abdomen were chosen to be subcutaneously injected with PEG-DTTC-TNBs, PEG-DTDC-TNBs, PEG-O170-TNBs (in 1X PBS, PH = 7.4) solution and nothing, respectively. The Raman spectra of the four places were detected with the Raman spectrometer. Another mouse was treated with a tail vein injection with PEG-DTTC-TNBs solution. 3 h later, the mouse was anesthetized and Raman spectra of three locations in the liver, one in the lung and one in the intestinal tract, were measured with the Raman spectrometer. Herein, the Raman probe must attach

to the skin tightly to ensure that the excitation light is focused into the internal organs.

2.5. Laser Ablation

This experiment was carried out through pulsed laser ablation. 640 nm AuAg TNBs coated with PEG were prepared. The solution was centrifuged to remove excess PEG and water and then dispersed and dried on ITO glass. The sample was ablated by a femtosecond Ti:Sapphire laser (Mai Tai HP). The laser was tuned to the NIR region (2.5 W, 800 nm, 100 fs, 80 MHz) to excite two-photon luminescence (TPL) from AuAg alloyed TNBs. We examined TPL imaging of triangular nanoboxes by confocal microscope (OLYMPUS FV1000, LSM). Emission was collected by a 60x oil-immersion objective (N.A. = 1.35) and a bandpass filter with a transmission window from 488 nm to 546 nm. The laser beam was focused on the sample with a spot size about 100 μm in diameter. The transmissivity of laser was firstly set to 10% for TPL examination and then to 30% for laser ablation. During the ablation, the sample was exposed to the laser light by 30s leading to that most of the TPL vanished.

3. RESULTS AND DISCUSSION

3.1. Synthesis and Characterization of AuAg Alloyed TNBs

Figure 1(a) illustrates the formation of AuAg alloyed TNBs. PSSS and citrate will influence the defect structure of the seeds, which predisposes them to grow into NPs [15]. The formation of AuAg alloyed TNBs includes three major steps [19]. (1) A large hole appears due to initiation of galvanic replacement and nanoframes form. (2) Coreduction of AuCl_4^- and Ag^+ generated by galvanic replacement results in formation of AuAg alloyed layer in the hole. Meanwhile, the alloyed layers also deposit on the edges. (3) As reaction proceeds, the hole is closed and an AuAg alloyed shell around a cavity forms. The Au/Ag ratio is 4 : 1 as that of reactants and some of the Ag will be present in the form of AgCl due to large amount of Cl^- in the solution. By changing the amount of seeds, Ag NPs with different sizes (P1–P4) were synthesized.

Figure 1(b) shows that the LSPR extinction spectra position of P1–P4 is at 495, 580, 680, 820 nm and corresponding TNBs (B1–B4) at 560, 640, 704 and 823 nm, respectively. The TEM images Figs. 1(c)–(f) shows that the yield of Ag NPs is over 95% with only a few rod or sphere shapes. In sample P1, most are round plate shapes while triangular plate shapes in sample P2–P4. Based

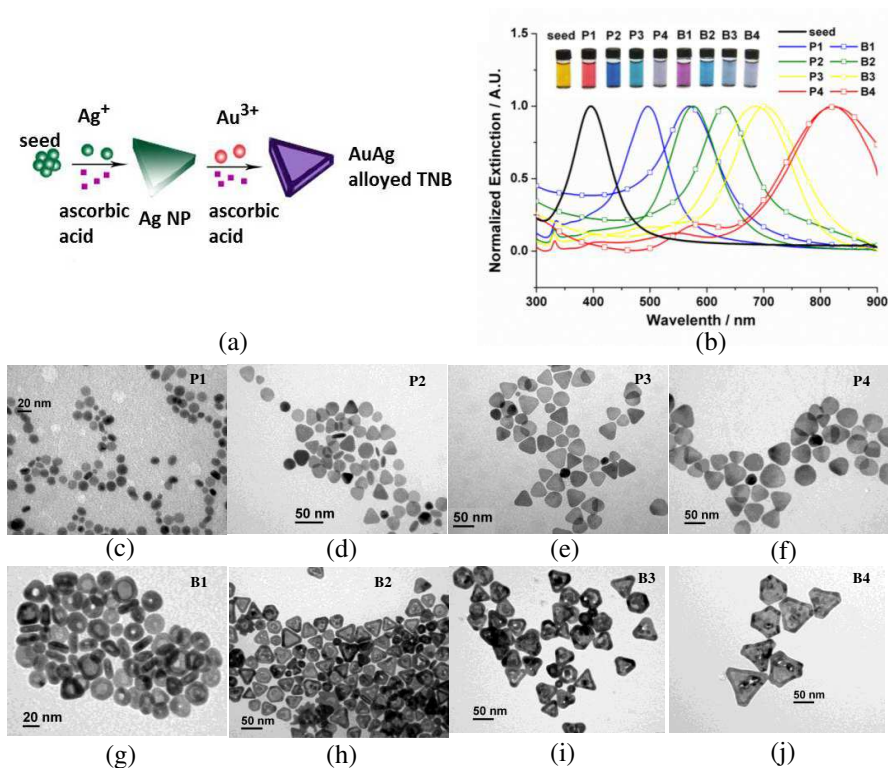


Figure 1. (a) Schematic diagram illustrating the preparation of AuAg alloyed TNBs. (b) The extinction spectra of seed, Ag Nanoprisms (P1–P4) at 495, 580, 680 and 820 nm and corresponding AuAg alloyed TNB (B1–B4) at 560, 640, 704 and 823 nm, respectively. (c)–(j) are TEM images of P1–P4 (c)–(f) and B1–B4 (g)–(j) in (b).

on these templates, sample B1 has many round plate-like triangular nanoboxes and the mass in sample B2–B4 are TNBs as shown in Figs. 1(g)–(k). This indicates that the shape of TNBs highly depends on that of the Ag templates. Fig. 2 shows the averaged size data of nanoparticles measured from several TEM images. The perpendicular length was measured from the flat-lying NPs and TNBs while the thickness value was obtained from some vertically oriented ones. Both the perpendicular length and thickness of internal cavities are smaller than that of the original templates.

This small decrease can be explained by the etching process of the Ag layer in the first step before alloying [19]. The UV-vis spectra of AuAg alloyed TNBs are red shift, in contrast with Ag NPs, resulting

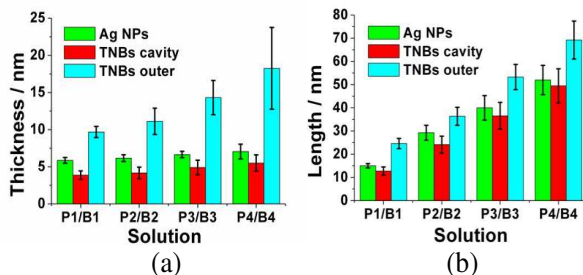


Figure 2. The size data of length and thickness of Ag NPs P1–P4 and TNBs B1–B4 (cavity and outer) measured from several TEM images by averaging.

from core-shell structure formation as well as an increase in the Au/Ag ratio and particle volume, which have been demonstrated in AuAg alloyed nanospheres [24], nanocages [25], and nanoframes [26]. As the volume of TNBs increases, the red shift value decreases. Almost no increment exists from sample P4 to sample B4. This can be explained by the faster increase of thickness than edge length during the process of TNBs formation resulting in a relative decrease in the aspect ratio of the lateral length to thickness. The decrease in the aspect ratio causes a blue shift, which counteracts the red shift due to structure and composition changes. The extinction spectra position of sample B1–B4 is 560, 640, 704 and 823 nm, respectively. Due to the optical feature of vast tunable LSPR band, AuAg alloyed TNBs might have great potentials as substrate for index sensing, SERS, SEF and fluorescence quenching (FQ) research, or as contrast agents for optical coherence tomography and photoacoustic imaging. In experiment, we found that the peak values of the LSPR spectra of all TNB samples are all almost double that of Ag NPs at the same level of concentration.

3.2. FDTD Calculations

As estimation of the SERS enhancement factor, the electrodynamics of nonspherical metal nanoparticles has long been of interest. However, there are very few analytical theory results for AuAg alloyed TNBs. The finite difference time domain (FDTD) method is a popular computational electrodynamics modeling technique. FDTD is a fully vectorial method. The electromagnetic fields and structural materials of interest are described on a discrete mesh made up of so-called Yee cells. Maxwell's equations are solved discretely in time, where the time step used is related to the mesh size through the speed of light.

Table 1. Sizing data of length and thickness of the whole nanoparticle and interior cavity obtained from TEM measurements for **B1–B4**.

Sample	Outer length [nm]	Outer thickness [nm]	Cavity length [nm]	Cavity thickness [nm]
B1	24.6 ± 2.2	9.7 ± 0.7	12.7 ± 1.8	3.9 ± 0.6
B2	36.4 ± 3.8	11.1 ± 1.8	24.1 ± 3.7	4.2 ± 0.8
B3	53.3 ± 5.4	14.3 ± 2.3	36.6 ± 5.8	4.9 ± 1.1
B4	69.2 ± 8.2	18.2 ± 5.5	49.5 ± 7.4	5.5 ± 1.1

In this section, we have modeled an AuAg alloyed hollow (water-filled) nanobox structure for sample B1–B4 by Lumerical FDTD Solutions software. The dimensions of each model are based on the TEM analysis as shown in Table 1. The ends of all tips of the triangular nanoboxes have been rounded by a cylinder with a radius of 5 nm to fit better the structures observed in the TEM images. All calculations refer to pure water as the external dielectric medium. Herein, we assume that AuAg alloyed TNBs are composed by uniformed AuAg alloyed materials. Nanoboxes are modeled by a composition-weighted linear combination of the dielectric functions of the metals [17]. The Au/Ag ratio, 4 : 1 in our simulation, is determined by the amounts of metallic Ag and Au in reactions, such that:

$$\varepsilon_{\text{alloyed}} = (4 \cdot \varepsilon_{\text{Au}} + \varepsilon_{\text{Ag}})/5 \quad (1)$$

The dielectric constant of Au and Ag are taken from Palik [27].

Material parameter curve fitting is done automatically by Lumerical software. The mesh size is 0.5 nm in and around the structure, and 10 nm is the maximum mesh size elsewhere. The source is a Total Field Scattered Field (TFSF) plane wave, which is especially useful for single structures since it is little influenced by tiny reflections from the perfect match layer (PML). The polarization vector is typically taken in the parallel directions to the perpendicular length of the triangle, while the direction of the k -vector is taken to be perpendicular to the plane of the structure. Herein, we calculated the wavelength-dependent curve of the E -field enhancement factor. The E -field enhancement contours both through the particle center and on the surface are plotted. All calculations are converged and stopped when the value of autoshutoff reaches 10^{-6} .

The results of the FDTD calculations are given in Fig. 3. For the E -field enhancement, only the data point between 300 nm and 900 nm are shown for clarity. A full list of all parameters is shown in Table 2. For nanobox structure, the E -field enhancement is sensitive

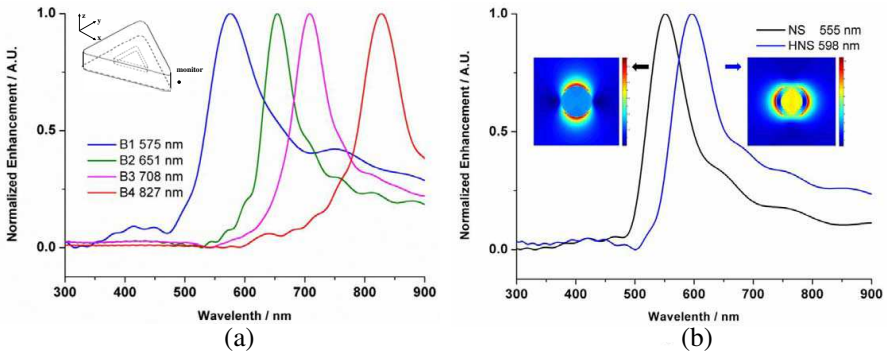


Figure 3. The calculated E -field enhancement of (a) the AuAg alloyed TNBs for B1–B4 based on TEM data in Table 1, and (b) the 35 nm-diameter Au nanosphere (NS) and hollow AuAg nanosphere (HNS) with 5 nm shell thickness. The E -field enhancement contours of both the NS and HNS are shown in the inset of (b).

Table 2. Parameters for FDTD calculations of AuAg alloyed TNBs B1–B4.

Sample	Outer length [nm]	Outer thickness [nm]	Cavity length [nm]	Cavity thickness [nm]	Ag [%]	Au [%]
B1	22	18	8	3	20	80
B2	32	13	21	3	20	80
B3	50	17	36	5	20	80
B4	62	15	55	7	20	80

to its outer length, cavity length, outer thickness and cavity thickness. The long wavelength dipole resonance is obviously red-shifted when the outer/cavity length is increased. However, the variation in outer/cavity thickness between the samples is not statistically significant. The calculated E -field enhancement in Fig. 3(a) of the AuAg alloyed triangular nanoboxes show a perfect match to the experimental results. Fig. 4 presents E -fields enhancement contours external to triangular nanoboxes in Fig. 3(a), all for their longest wavelength plasmon resonance respectively. The calculations show that the maximum enhancement for the dipole resonances occurs at the particle tips (see arrows in Fig. 4) along the polarization vector. The largest electric fields ($|E|^2$) at their peak resonance wavelength are 80 for B1, 746 for B2, 1997 for B3, 2906 for B4 in the plane through the particle

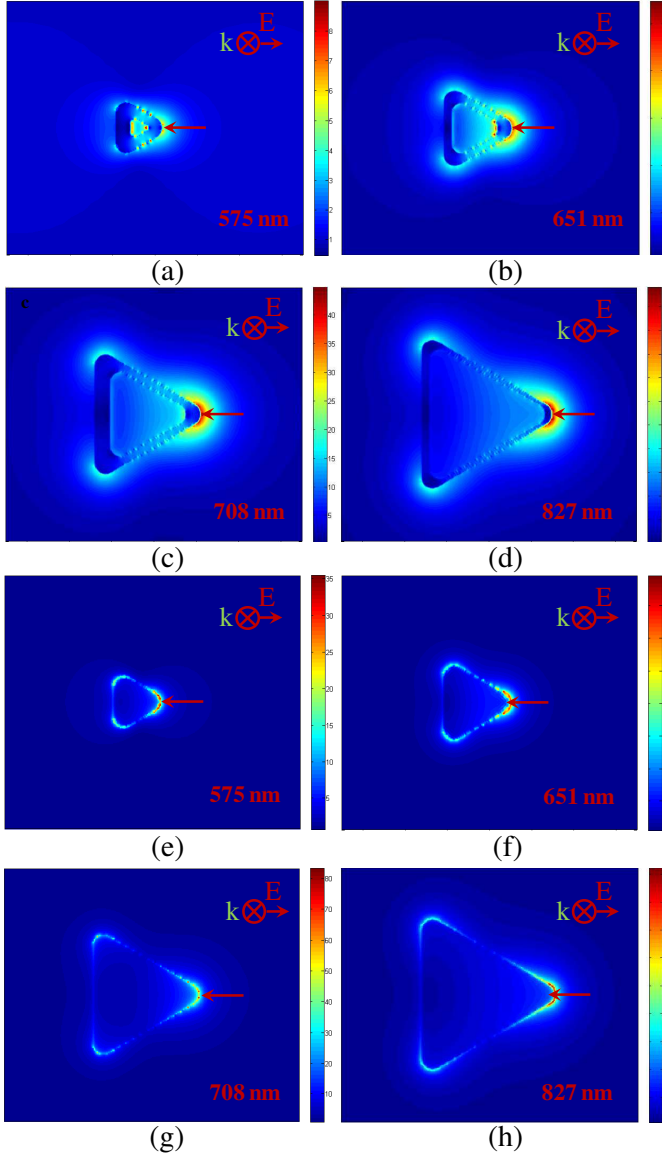


Figure 4. Is the E -field enhancement contours of sample B1–B4 at corresponding resonance wavelengths. Both the E -fields through the particle center (a)–(d) and on the surface (e)–(h) are plotted. The polarization direction is along their perpendicular length of the triangle. The red arrows show where the maximum value of the E -field is.

center, and 1225, 6240, 6889, and 8464 on the corresponding upper surface of the nanostructures, respectively. Compared to 555 nm peak excitation for Au nanosphere and 598 nm peak excitation for hollow AuAg nanospheres in Fig. 3(b), the triangular nanobox shows an obviously stronger enhanced local electric field.

3.3. In Vivo SERS Detection of PEG-dyes-TNBs Tags

To study the relationship of Raman enhancement with metallic nanoparticles, AuAg alloyed triangular nanoboxes conjugated with three kinds of dye molecules (DTTC, DTDC and O170) were prepared as SERS tags. Based on a previous study [28, 29], 643 nm metallic nanoparticles produced the strongest Raman signal under 785-nm laser excitation, because of the difference in laser absorption competition between nanoparticles and absorbed Raman molecules as well as the difference in reabsorption of Raman emission by different nanoparticles. As a result, 640 nm TNBs were used for the SERS tags.

Figure 5 shows the Raman spectra of PEG-dyes-TNBs tags in solution based on 640 nm TNBs, as well as the extinction spectra of the SERS tags at each step during the synthesis process. Three dyes (DTTC, DTDC and O170) were used in our experiment.

As we can see, SERS intensity of the dyes was remarkably enhanced by the local field of triangle nanoboxes. The vibration bands of the dyes are also clearly shown in this figure. For the extinction spectra, the spectrum of TNBs red-shifted 8 nm after dyes and PEG coating, because of the following three reasons: First, the coating has larger refractive index compared to water, and the LSPR band of TNBs is very sensitive to the refractive index of their surrounding medium. Second, the distinction spectrum of PEG-TNBs solution is broadened, because the Cross-linking effect [30] of PEG leads to the agglomeration of TNB particles. Third, the spectrum peaks of the dyes are larger than TNBs (640 nm), so a little red shift is expected. As a result, both the red shift and broadening of the spectrum implicate that the surface of TNBs have been fully coated by dye-PEG.

Then, 20 μ L of each tag was subcutaneously injected into mice skin at area A (DTTC), B (DTDC) and C (O170) respectively, while D area was injected with pure PBS solution for comparison. For SERS imaging, all the areas were irradiated with 785 nm laser line. Raman spectra of the whole area were measured with a Raman spectrometer (BWTEK), as shown in Fig. 6. Under 785 nm laser excitation, the obtained SERS spectrum (Figs. 6(b)–(e)) of each sample was the same as the corresponding SERS tags in the solution Figs. 6(b)–(d) showed the characteristic Raman fingerprint of DTTC, DTDC and O170 respectively, while Fig. 6(e) didn't show any Raman signals.

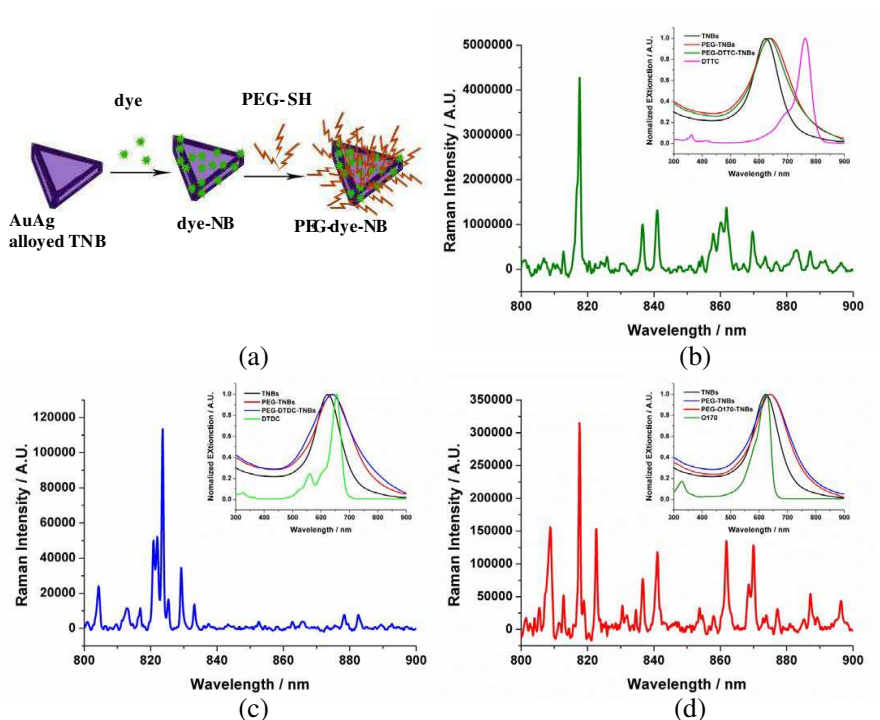


Figure 5. (a) Schematic diagram illustrating the preparation of PEG-dyes-TNBs SERS tags based on 640 nm AuAg alloyed TNBs. (b)–(d) Are the Raman spectra of PEG-DTTC-TNBs, PEG-DTDC-TNBs, PEG-O170-TNBs measured in solution respectively. The graphs in the upper right corner are the corresponding extinction spectra of the SERS tags at each step during the synthesis process.

We further treated another mouse with a tail vein injection with PEG-DTTC-TNBs solution. 3 h later, the Raman spectra of one location in the lung (A), three in the liver (B, C and D), and one in intestinal tract (E) were measured. As shown in Fig. 7, the Raman intensity in the liver where most of the SERS tags were deposited was significantly stronger than that of both lung and intestinal tract.

3.4. Femtosecond Laser Near-field Ablation

Using magnetic nanostructures as drug delivery carriers is a promising research subject in biomedical applications [31]. Typically, magnetic nanoparticles is used for drug delivery by utilizing polymers

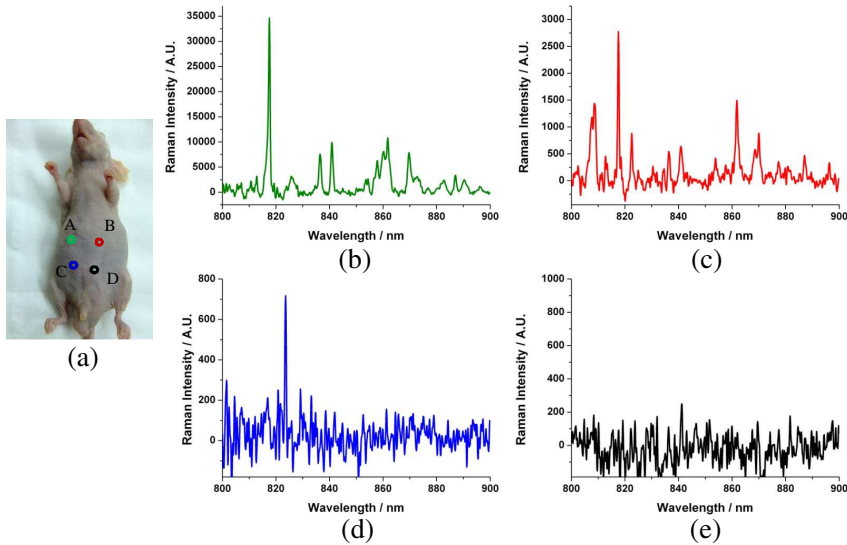


Figure 6. Raman spectra of mice skin. (a) Photograph of mice. The red circled areas A–D were subcutaneously injected with PEG-DTTC-NBs, PEG-DTDC-NBs, PEG-O170-NBs solution and PBS solution only, respectively. (b)–(e) Are Raman spectra at the center of area A, B, C and D respectively.

to coat magnetic nanoparticles and encapsulate drugs to form nanocapsules [32], which may need complicated processes and result in modest efficiency.

However, the unique properties of AuAg hollow structures give an example of a novel drug delivery system that uses the nanoparticles to directly encapsulate the potential anticancer drug without any surface coating. One possible method to release the drug encapsulated inside the hollow structure is laser-induced fragmentation of the hollow structure [33]. The concept of using pulsed lasers to affect the structure of metal nanoparticles has been studied before [34–38]. Under fs laser irradiation, the AuAg alloyed TNBs were broken down into small nanoparticles, which is a potential application to controlled drug delivery. In our experiment, we detected the two-photon luminescence (TPL) intensities of AuAg alloyed TNB irradiated by fs 800 nm laser, so as to monitor the laser ablation process. By adjusting the illumination time, TPL intensities of the triangular nanoboxes were dropped by over 80% (see Figs. 8(a), (b)). In this case, we assumed that most of the triangular nanoboxes were ablated. The morphology of the

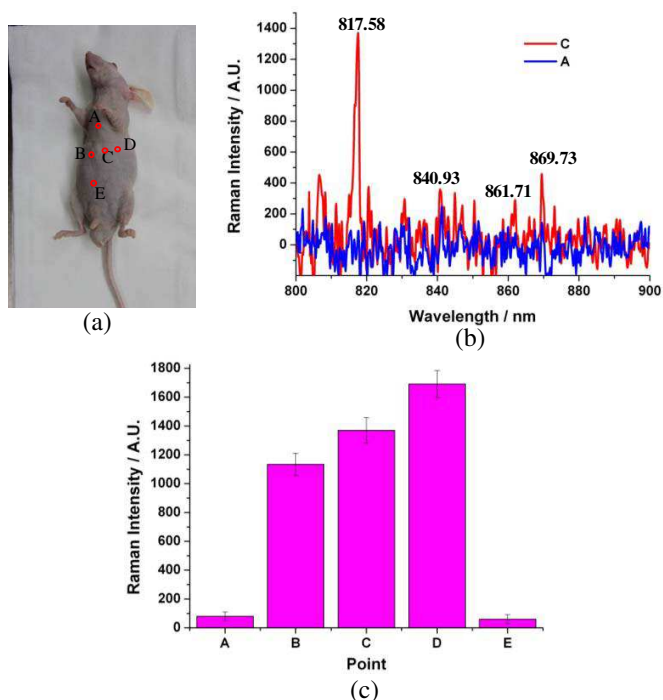


Figure 7. Raman spectra of deep tissue in mice. (a) Photograph of mice. Liver is under the red circuted area B, C and D. (b) Raman spectra under the center of area A and C. (c) Raman intensity at 817.58 nm under different areas.

samples was observed by scanning electron microscopy (SEM). As shown in Figs. 8(c), (d), the triangular nanoboxes were ablated into small nanoparticles, most of which were nanospheres. Herein, we also found the TPL efficiency of hollow triangular nanoboxes much higher than that of nanospheres.

Based on Wheeler's study [39], there are two possible processes behind the laser-induced fragmentation: (i) conversion of big hollow nanoparticles to smaller and hollow nanoparticles, and (ii) breakdown of big hollow nanoparticles into smaller but solid nanoparticles directly. Process (i) becomes more dominant over process (ii) at higher laser peak power. However, there are some 100 nm-diameter nanoparticles observed in Fig. 8(d), which are larger than original triangular nanoboxes. We hypothesis the large nanoparticles could be induced by the fusion of smaller hollow nanoparticles and/or solid nanoparticles with each other under laser illumination.

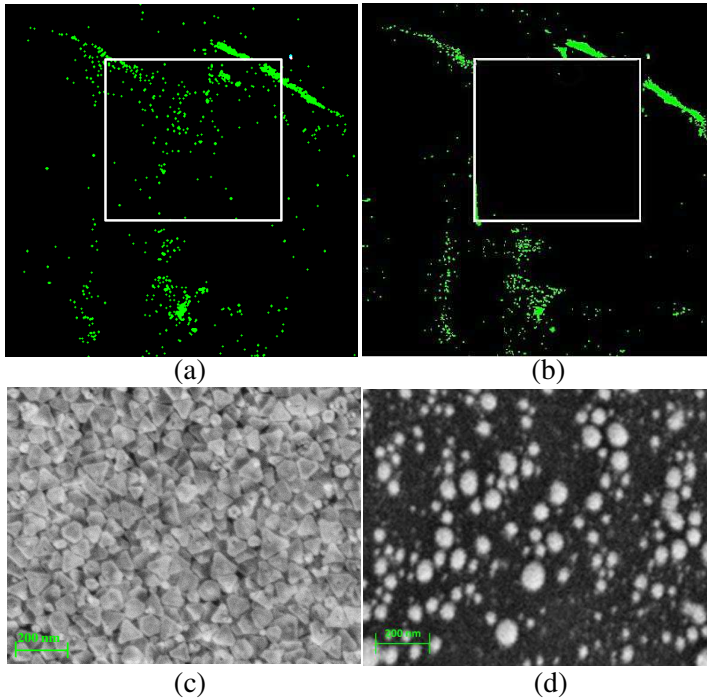


Figure 8. Shows the TPL images of AuAg alloyed TNBs before (a) and after (b) laser-induced fragmentation. The bright spots are considered to be produced by clusters of AuAg alloyed TNBs. The sample (in the white box) was illuminated for 30s leading to the TPL intensity to drop by 80%. (c)–(d) Show the morphology of AuAg alloyed TNBs on ITO glass before (c) and after (d) laser ablation observed by SEM (CARL ZEISS ULTRA55).

4. CONCLUSION

In summary, we systematically studied the surface plasmon properties of hollow AuAg alloyed triangular nanoboxes. Four kinds of AuAg alloyed triangular nanoboxes (TNBs) with LSPR spectra position from visible to NIR region were successfully synthesized. FDTD calculations were conducted for the first time to study the optical properties of individual particles of AuAg alloyed TNBs. The calculated E -field enhancement was excellent agreed with the experimental result which displayed significant sensitivity to the outer length and thickness size of the nanostructures. We further plotted the E -field, external to four kinds of AuAg alloyed TNBs, and found that the largest $|E^2|$

values of TNBs are increased with their size and obviously larger than that of Au nanospheres. Since the E -field enhancement factor is important in determining normal and single molecule SERS intensities, we synthesized three kinds of SERS tags based on AuAg alloyed TNBs and further applied them in “in vivo” SERS imaging. The TNBs were proved to be promising for multiplexed SERS imaging. In addition, the laser ablation study of AuAg alloyed TNBs indicated that the unique hollow structure of these nanoparticles are potential for directly controlled drug delivery in the future.

ACKNOWLEDGMENT

This work was supported by the National Nature Science Foundation of China (No. 60978063 and No. 61008052), the Fundamental Research Funds for the Central Universities, the Science and Technology Department of Zhejiang Province (2010R50007), the China Postdoctoral Science Foundation (20090461394) and AOARD. We also want to express our gratitude toward the Medical School of Zhejiang University for their supply of mice.

REFERENCES

1. Kelly, K. L., et al., “The optical properties of metal nanoparticles: The influence of size, shape, and dielectric environment,” *Journal of Physical Chemistry B*, Vol. 107, No. 3, 668–677, 2003.
2. Liaw, J.-W., M. K. Kuo, and C. N. Liao, “Plasmon resonances of spherical and ellipsoidal nanoparticles,” *Journal of Electromagnetic Waves and Applications*, Vol. 19, No. 13, 1787–1794, 2005.
3. Muhlschlegel, P., et al., “Resonant optical antennas,” *Science*, Vol. 308, No. 5728, 1607–1609, 2005.
4. Xie, H., F. M. Kong, and K. Li, “THE electric field enhancement and resonance in optical antenna composed of Au nanoparticles,” *Journal of Electromagnetic Waves and Applications*, Vol. 23, No. 4, 534–547, 2009.
5. Rand, B. P., P. Peumans, and S. R. Forrest, “Long-range absorption enhancement in organic tandem thin-film solar cells containing silver nanoclusters,” *Journal of Applied Physics*, Vol. 96, No. 12, 7519–7526, 2004.
6. Huang, X. H., et al., “Cancer cell imaging and photothermal therapy in the near-infrared region by using gold nanorods,”

- Journal of the American Chemical Society*, Vol. 128, No. 6, 2115–2120, 2006.
7. Yavuz, M. S., et al., “Gold nanocages covered by smart polymers for controlled release with near-infrared light,” *Nature Materials*, Vol. 8, No. 12, 935–939, 2009.
 8. Jain, P. K., et al., “Calculated absorption and scattering properties of gold nanoparticles of different size, shape, and composition: Applications in biological imaging and biomedicine,” *Journal of Physical Chemistry B*, Vol. 110, No. 14, 7238–7248, 2006.
 9. Anker, J. N., et al., “Biosensing with plasmonic nanosensors,” *Nature Materials*, Vol. 7, No. 6, 442–453, 2008.
 10. Jain, P. K., et al., “Noble metals on the nanoscale: Optical and photothermal properties and some applications in imaging, sensing, biology, and medicine,” *Accounts of Chemical Research*, Vol. 41, No. 12, 1578–1586, 2008.
 11. Noguez, C., “Surface plasmons on metal nanoparticles: The influence of shape and physical environment,” *Journal of Physical Chemistry C*, Vol. 111, No. 10, 3806–3819, 2007.
 12. Sau, T. K., et al., “Properties and applications of colloidal nonspherical noble metal nanoparticles,” *Advanced Materials*, Vol. 22, No. 16, 1805–1825, 2010.
 13. Millstone, J. E., et al., “Observation of a quadrupole plasmon mode for a colloidal solution of gold nanoprisms,” *Journal of the American Chemical Society*, Vol. 127, No. 15, 5312–5313, 2005.
 14. Millstone, J. E., G. S. Metraux, and C. A. Mirkin, “Controlling the edge length of gold nanoprisms via a seed-mediated approach,” *Advanced Functional Materials*, Vol. 16, No. 9, 1209–1214, 2006.
 15. Aherne, D., et al., “Optical properties and growth aspects of silver nanoprisms produced by a highly reproducible and rapid synthesis at room temperature,” *Advanced Functional Materials*, Vol. 18, No. 14, 2005–2016, 2008.
 16. Haes, A. J., et al., “Nanoscale optical biosensor: Short range distance dependence of the localized surface plasmon resonance of noble metal nanoparticles,” *Journal of Physical Chemistry B*, Vol. 108, No. 22, 6961–6968, 2004.
 17. Hao, E. and G. C. Schatz, “Electromagnetic fields around silver nanoparticles and dimers,” *Journal of Chemical Physics*, Vol. 120, No. 1, 357–366, 2004.
 18. Nelayah, J., et al., “Mapping surface plasmons on a single metallic nanoparticle,” *Nature Physics*, Vol. 3, No. 5, 348–353, 2007.

19. Aherne, D., et al., "From Ag nanoprisms to triangular AuAg nanoboxes," *Advanced Functional Materials*, Vol. 20, No. 8, 1329–1338, 2010.
20. Tong, L., et al., "Bright three-photon luminescence from gold/silver alloyed nanostructures for bioimaging with negligible photothermal toxicity," *Angewandte Chemie International Edition*, Vol. 49, No. 20, 3485–3488, 2010.
21. Chen, J. Y., et al., "Gold nanocages: Engineering their structure for biomedical applications," *Advanced Materials*, Vol. 17, No. 18, 2255–2261, 2005.
22. Kudelski, A., "Influence of electrostatically bound proteins on the structure of linkage monolayers: Adsorption of bovine serum albumin on silver and gold substrates coated with monolayers of 2-mercaptoethanesulphonate," *Vibrational Spectroscopy*, Vol. 33, Nos. 1–2, 197–204, 2003.
23. Qian, X. M., et al., "In vivo tumor targeting and spectroscopic detection with surface-enhanced Raman nanoparticle tags," *Nature Biotechnology*, Vol. 26, No. 1, 83–90, 2008.
24. Link, S., Z. Wang, and M. El-Sayed, "Alloy formation of gold-silver nanoparticles and the dependence of the plasmon absorption on their composition," *The Journal of Physical Chemistry B*, Vol. 103, No. 18, 3529–3533, 1999.
25. Hu, M., et al., "Optical properties of Au-Ag nanoboxes studied by single nanoparticle spectroscopy," *Journal of Physical Chemistry B*, Vol. 110, No. 40, 19923–19928, 2006.
26. Metraux, G. S., et al., "Triangular nanoframes made of gold and silver," *Nano Letters*, Vol. 3, No. 4, 519–522, 2003.
27. Palik, E. D. (ed.), *Handbook of Optical Constants of Solids*, Academic Press, New York, 1998.
28. Jiang, L., et al., "Raman reporter-coated gold nanorods and their applications in multimodal optical imaging of cancer cells," *Analytical and Bioanalytical Chemistry*, Vol. 400, No. 9, 2793–2800, 2011.
29. Qian, J., et al., "Fluorescence-surface enhanced Raman scattering co-functionalized gold nanorods as near-infrared probes for purely optical in vivo imaging," *Biomaterials*, Vol. 32, No. 6, 1601–1610, 2011.
30. Li, X., J. Qian, and S. He, "Impact of the self-assembly of multilayer polyelectrolyte functionalized gold nanorods and its application to biosensing," *Nanotechnology*, Vol. 19, 355501, 2008.

31. Neuberger, T., et al., "Superparamagnetic nanoparticles for biomedical applications: Possibilities and limitations of a new drug delivery system," *Journal of Magnetism and Magnetic Materials*, Vol. 293, No. 1, 483–496, 2005.
32. Gupta, A. K. and M. Gupta, "Synthesis and surface engineering of iron oxide nanoparticles for biomedical applications," *Biomaterials*, Vol. 26, No. 18, 3995–4021, 2005.
33. Lu, W., et al., "Tumor site-specific silencing of NF-kappa B p65 by targeted hollow gold nanosphere-mediated photothermal transfection," *Cancer Research*, Vol. 70, No. 8, 3177–3188, 2010.
34. Link, S., et al., "Laser photothermal melting and fragmentation of gold nanorods: Energy and laser pulse-width dependence," *Journal of Physical Chemistry A*, Vol. 103, No. 9, 1165–1170, 1999.
35. Kamat, P. V., M. Flumiani, and G. V. Hartland, "Picosecond dynamics of silver nanoclusters. Photoejection of electrons and fragmentation," *Journal of Physical Chemistry B*, Vol. 102, No. 17, 3123–3128, 1998.
36. Kurita, H., A. Takami, and S. Koda, "Size reduction of gold particles in aqueous solution by pulsed laser irradiation," *Applied Physics Letters*, Vol. 72, No. 7, 789–791, 1998.
37. Inasawa, S., M. Sugiyama, and Y. Yamaguchi, "Laser-induced shape transformation of gold nanoparticles below the melting point: The effect of surface melting," *Journal of Physical Chemistry B*, Vol. 109, No. 8, 3104–3111, 2005.
38. Plech, A., et al., "Femtosecond laser near-field ablation from gold nanoparticles," *Nature Physics*, Vol. 2, No. 1, 44–47, 2006.
39. Wheeler, D. A., et al., "Optical properties and persistent spectral hole burning of near infrared-absorbing hollow gold nanospheres," *Journal of Physical Chemistry C*, Vol. 114, No. 42, 18126–18133, 2010.